Limnol. Oceanogr., 53(6), 2008, 2668–2680

Modeling flow in coral communities with and without waves: A synthesis of porous media and canopy flow approaches

Ryan J. Lowe[1]
School of Environmental Systems Engineering, University of Western Australia, Crawley, Western Australia, Australia

Uri Shavit
Civil and Environmental Engineering, Technion, Haifa, Israel

James L. Falter
Hawaii Institute of Marine Biology, University of Hawaii, Kaneohe, Hawaii, 96744

Jeffrey R. Koseff and Stephen G. Monismith
Civil and Environmental Engineering, Stanford University, Stanford, California 94305

Abstract

Both canopy flow and porous media theories have been developed independent of one another to predict flow through submerged porous structures. These approaches are very similar, albeit with some key differences in how canopy resistance forces are parameterized. Canopy models provide a means of parameterizing the shear stresses that occur at the top of the canopy, whereas porous media models can often provide a simpler and more tractable way of parameterizing turbulent form drag based on simple morphological metrics and empirical relationships already in the hydrology literature. We developed a set of equations combining aspects of both models and applied this hybridized model to predict the flow structure within an experimental canopy formed by the branching coral *Porites compressa*, using model parameter values obtained from the literature. Results from the model predictions agreed well with direct measurements of flow speed and flow forces derived from particle image velocimetry under conditions of both unidirectional and wave-driven oscillatory flow.

The flow structure within benthic boundary layers can have important consequences on the ecology of benthic organisms and in turn how these organisms affect the hydrodynamics occurring within their environment. Early boundary layer models of turbulent, unidirectional flow over solid walls describe three distinct regions: a viscous sublayer, a logarithmic layer, and an outer layer (Schlichting and Gersten 2000). This simple, universal model has been successful in describing turbulent flow over various naturally rough bottoms (Raupach et al. 1991). However, the roughness of many bottoms is large enough to be more accurately described as submerged "canopy flows" (Nepf and Vivoni 2000). The use of the term "canopy" reflects the similarity these flows have to atmospheric flows over terrestrial canopies (Finnigan 2000). What distinguishes canopy flow models most from conventional boundary layer models are that (1) they describe the flow within the roughness elements, and (2) they include an inflection point in the mean velocity profile that leads to the generation of instabilities that enhance turbulent exchange between the canopy and the overlying water column (Ackerman and Okubo 1993; Ghisalberti and Nepf 2002).

For both terrestrial canopies and aquatic canopies where the water depth is much greater than the canopy height (i.e., unconfined flow conditions), the shear stress at the top of the canopy is the dominant force driving flow inside the canopy and is opposed by form drag exerted by the canopy elements (Raupach et al. 1991). This shear-driven transfer of momentum to the canopy interior becomes less important as the water depth becomes shallow with respect to the canopy height; in this case, the flow becomes confined, also termed "depth limited" (Nowell and Church 1979; Nepf and Vivoni 2000). For shallow flows (i.e., those approaching "emergent" conditions), the contribution of boundary layer shear becomes negligible since the primary momentum balance is instead between the external pressure gradient and form drag (Nepf and Vivoni 2000). This transition results in greater flow within the canopy than would otherwise occur under unconfined conditions (Wu et al. 1999; Mcdonald et al. 2006).

Analogous to confined unidirectional canopy flow, the shear-driven transfer of momentum to the interior of a canopy also becomes less important when they are subjected to wave-driven oscillatory flow. Under typical wave conditions, pressure-driven flow accelerations are balanced mostly by the form drag and inertial forces

[1] Corresponding author (ryan.lowe@uwa.edu.au).

Acknowledgments

We thank Marlin Atkinson for helping to inspire this work and for providing the coral skeletons used in the experiments as well as thank Katie Fitzgibbons for assisting with the coral roughness and porosity measurements. Finally, the authors are grateful for the comments from the reviewers who helped improve both the content and the clarity of the paper. This research was supported by grant OCE-0117859 from the National Science Foundation. RJL acknowledges support from an Australian Research Council Discovery Project grant DP0770094.

exerted by the canopy elements, with shear at the top of the canopy playing only a minor role (Lowe et al. 2005*b*). This also results in greater in-canopy flow than for unconfined, unidirectional flow. Therefore, for both confined flows and wave-driven oscillatory flows, shear-dependent models of momentum transfer are no longer valid and will fail to correctly predict flow inside a canopy.

Greater in-canopy flow under either confined or oscillatory flow also results in higher rates of frictional dissipation than under unconfined unidirectional flow (Lowe et al. 2007). This is particularly important given that frictional dissipation can play a major role in the transformation of waves propagating inshore when the bottom is naturally very rough, that is, over rocky bottoms (e.g., Adams et al. 2002), aquatic vegetation (e.g., Mendez and Losada 2004), or coral reefs (e.g., Lowe et al. 2005*a*). Flow within living canopies can also be important to benthic communities (Carpenter et al. 1991; Atkinson and Bilger 1992; Lesser et al. 1994). For example, under oscillatory flow, nutrient uptake by corals can be twice as fast as under unidirectional flow as a result of the greater in-canopy flow generated (Lowe et al. 2005*c*; Reidenbach et al. 2006*a*).

Modeling flow within submerged canopies can be challenging because of the complex morphologies that benthic organisms form. Flow properties will thus vary spatially in a canopy, leading to so-called mechanical dispersion, for example, due to the tortuosity of the flow paths and wakes behind the roughness elements. Because it is nearly impractical to directly model these microscopic spatial flow variations, "macroscopic" continuum approaches are instead used where only spatially averaged flow properties are directly considered and microscale variations are accounted for using some closure scheme. Following what is done in unidirectional canopy flow models, Lowe et al. (2005*b*) developed such a model for predicting wave-driven oscillatory flow within canopies by parameterizing canopy forces as a function of canopy geometry, in their case an array of vertical cylinders. For certain types of canopies, such as seagrasses (Nepf and Vivoni 2000), forests (Finnigan 2000), and buildings (Britter and Hanna 2003), values for these geometric parameters can be readily assigned. Unfortunately, the morphology of many natural canopies may be too complex to be represented by a simple set of geometric parameters analogous to a cylinder array. For example, the coral bed shown in Fig. 1 has some properties of such a canopy (e.g., the corals have cylindrical branches), but the overall geometry is fundamentally complex and three-dimensional (3D).

The development of porous media theory, however, was specifically motivated by the need to predict flow inside naturally complex, 3D porous matrices of varying composition. Unlike canopy flow theory, in which flow between the roughness is assumed to be turbulent, porous media theory generally assumes that the flow is laminar (i.e., governed by Darcy's law). Nonetheless, Oldham and Sturman (2001) applied porous media theory to predict turbulent unidirectional flow through emergent vegetation. Sollitt and Cross (1972) developed a model of turbulent flow through emergent permeable breakwaters that Gu and Wang (1991) later modified to model wave-driven flow through submerged porous beds. The Gu and Wang (1991) model is dynamically similar to existing canopy flow models when form drag inside a canopy dominates over laminar resistance. Thus, canopy and porous media flow theories assume similar momentum balances, although they differ in how they parameterize the resistance of flow within a canopy to external forcing. This difference can often be profound in terms of the greater tractability of porous media models over canopy models.

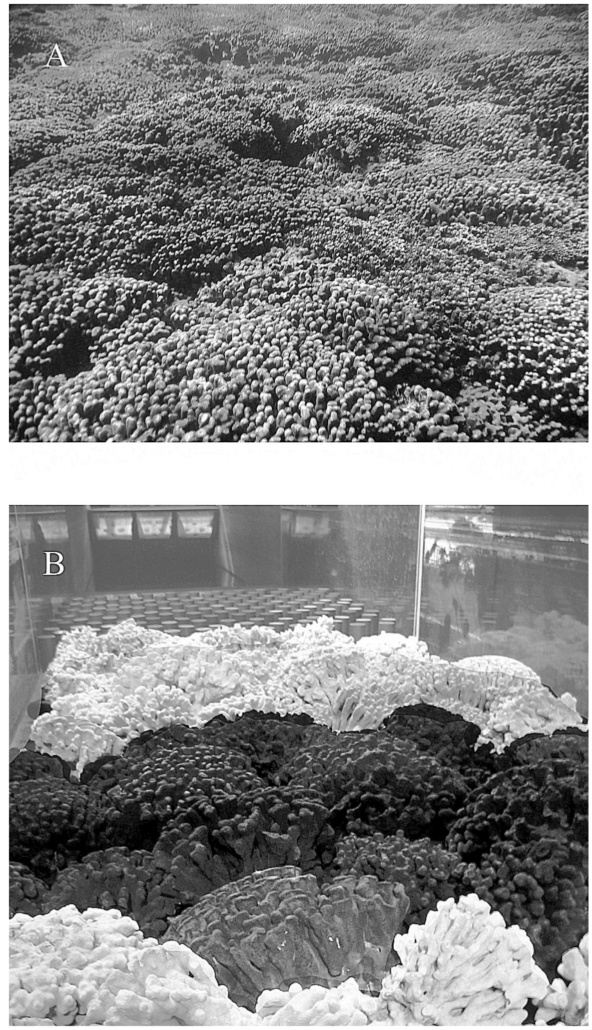

Fig. 1. (A) *Porites compressa* in Kaneohe Bay, Oahu, Hawaii (from Lowe et al. 2005*b*). (B) An experimental reef using *Porites compressa* skeletons in a wave-current flume looking upstream. Note that the black corals were painted with flat enamel paint to minimize laser light reflections.

In this paper, we present a hybridized model using concepts from both canopy and porous media theories to predict flow within canopies for both unidirectional and wave-driven flows. To our knowledge, no comparable model has been developed or tested on a naturally complex submerged canopy. Our combined model accurately describes changes in the mean canopy flow based on simple relationships between the model parameters, the morphology of the canopy, and the nature of the free-stream flow conditions. Although we test the model on an experimental canopy of branching coral, the approach of the model should be applicable to the broader physics of flow within submerged canopies.

Background: Canopy flow and porous media theory

Canopy flow theory—Lowe et al. (2005*b*) developed theory to predict flow within a submerged canopy that is valid under both unidirectional and oscillatory flow. The canopy consisted of an array of vertical cylinders of height h_c, diameter d, and spacing S. The momentum equation governing the spatially averaged (excluding the solid elements) in-canopy velocity $\hat{U}_w$ was

$$\underbrace{\frac{d\hat{U}_w}{dt}}_{\text{local acceleration}} = \underbrace{-\frac{1}{\rho}\frac{dP}{dx}}_{\text{pressure gradient}} + \underbrace{\frac{C_f}{2h_c}|U_{\infty,w}|U_{\infty,w}}_{\text{shear stress}} - \underbrace{\frac{C_d\lambda_f}{2h_c(1-\lambda_p)}|\hat{U}_w|\hat{U}_w}_{\text{form drag}} - \underbrace{\frac{C_M\lambda_p}{1-\lambda_p}\frac{d\hat{U}_w}{dt}}_{\text{inertial force}} \tag{1}$$

where C_f, C_d, and C_M are empirical coefficients defined below. In Eq. 1, the left term represents a local flow acceleration, whereas each term on the right represents a force per unit canopy fluid mass that drives or resists the flow. The canopy geometry is represented by h_c and two other parameters: (1) λ_f, defined as the ratio of the total frontal area of the canopy elements to the total plan area occupied by the canopy, and (2) λ_p, defined as the ratio of the plan area occupied by the canopy elements to the total plan bed area (exposed bed + canopy elements) (Lowe et al. 2005*b*).

Lowe et al. (2005*b*) assumed that the free stream velocity $U_{\infty,w}$ was

$$U_{\infty,w}(t) = U_{\infty,w}^{\max}\cos\left(\frac{2\pi t}{T}\right) \tag{2}$$

where $U_{\infty,w}^{\max}$ is the velocity amplitude (independent of elevation z) and T is the period. Thus, the case $T \rightarrow \infty$ represents steady, unidirectional flow. Sufficiently high above the canopy, acceleration is balanced by a pressure gradient $\partial P/\partial x$:

$$\frac{\partial U_{\infty,w}}{\partial t} = -\frac{1}{\rho}\frac{\partial P}{\partial x} \tag{3}$$

This pressure gradient exists both above and below the canopy, thereby providing a mechanism to drive flow within the canopy. In addition to pressure gradients, shear stresses at the top of the canopy can also transfer momentum vertically into the canopy. Lowe et al. (2005*b*) parameterized this shear stress using a quadratic friction law based on $U_{\infty,w}$ and a friction coefficient C_f. They assumed that flow in the canopy is attenuated by drag and inertial forces exerted by individual canopy elements; these forces are modeled using Morison's equation (Dean and Dalrymple 1991) with empirical canopy drag C_d and inertia C_M coefficients.

To quantify the reduction of the in-canopy flow, Lowe et al. (2005*b*) defined an attenuation parameter α_w as the ratio of the root-mean-squared (rms) in-canopy wave velocity to the rms above-canopy velocity, that is,

$$\alpha_w \equiv \frac{\hat{U}_w^{rms}}{U_{\infty,w}^{rms}} \tag{4}$$

The Lowe et al. (2005*b*) model predicts that as the excursion length $A_\infty = U_{\infty,w}^{rms}T/2\pi$ of an oscillatory flow increases above a canopy, α_w will decrease to a minimum value $\alpha \equiv \hat{U}_c / U_{\infty,c}$ associated with an *unconfined* unidirectional flow, where $\hat{U}_c$ and $U_{\infty,c}$ are the unidirectional current speeds within and above the canopy, respectively.

Porous media theory—Gu and Wang (1991) proposed a model to predict flow induced by surface waves within a porous bed of thickness h_c. The bed was assigned a porosity ε (the fluid volume fraction) that is directly related to λ_p ($\lambda_p = 1 - \varepsilon$). For a depth-uniform oscillatory flow (i.e., when $h_c/L << 1$, in which L is the wavelength), the Gu and Wang (1991) model predicts that $\hat{U}_w$ within a bed is governed by an equation similar to Eq. 1:

$$\underbrace{\frac{d\hat{U}_w}{dt}}_{\text{local acceleration}} = \underbrace{-\frac{1}{\rho}\frac{dP}{dx}}_{\text{pressure gradient}} - \underbrace{\frac{\nu(1-\lambda_p)}{K_p}\hat{U}_w}_{\text{laminar resisting force}} - \underbrace{\beta|\hat{U}_w|\hat{U}_w}_{\text{form drag}} - \underbrace{\frac{C_M\lambda_p}{1-\lambda_p}\frac{d\hat{U}_w}{dt}}_{\text{inertial force}} \tag{5}$$

Flow within the porous structure is opposed by three forces. The "inertial force" term is formulated exactly as in the canopy model (Eq. 1). The "laminar resisting force" and "form drag" terms are derived from the Forchheimer equation (Whitaker 1996), which is used to model resistance in porous media. The Forchheimer equation is an extension of Darcy's law, in which the only force balance is between a pressure gradient and the laminar resisting force. Darcy's law is applicable only when the porous media Reynolds number ($\mathrm{Re}_p = U_p d/\nu$) is less than order one (Bear 1972), where U_p represents the intrinsic velocity and d represents a pore-size length scale. The "laminar resisting force" term in Eq. 5 is a function of the permeability (K_p, units m^2), which is determined by the internal geometry of the porous bed. The pore-size length scale d is generally estimated as $\sqrt{K_p}$ (Bear 1972). At higher Reynolds numbers, the flow in the bed becomes turbulent, and resistance is dominated by the form drag of the bed material. Similar to the form drag term in the canopy model, the Forchheimer correction is modeled using a quadratic drag law, where β is a dimensional drag parameter that is a function of the internal bed geometry.

Various models have been developed to relate K_p and β to geometric properties of a porous bed (Engelund 1953; Ward 1964; Sollitt and Cross 1972). Macdonald et al. (1979; hereinafter MEMD79) compiled data from a wide range of experiments made up of a variety of materials, such as spheres, cylinders, and fibrous mats, and proposed the ''modified Ergun equations'':

$$K_p = \frac{D_{eq}^2 \left(1 - \lambda_p\right)^3}{a_0 \lambda_p^2} \tag{6}$$

$$\beta = \frac{b_0 \lambda_p}{D_{eq}\left(1 - \lambda_p\right)} \tag{7}$$

where a_0 and b_0 are empirical constants and D_{eq} is a characteristic length scale of the porous medium. MEMD79 defined D_{eq} as an ''equivalent mean sphere diameter'' equal to six times the volume-to-surface ratio of the dominant particles making up the bed, for example, $D_{eq} = D_{sph}$ for a bed of spheres with diameter D_{sph}, and $D_{eq} = 1.5D_{cyl}$ for beds comprised of cylindrical fibers having diameter D_{cyl}. Using $a_0 = 180$ and $b_0 = 1.8$, they were able to predict K_p and β to within $\pm 50\%$ for all experimental data they considered. Although this is a large margin of uncertainty, we show below, via a sensitivity analysis, that under typical wave conditions, a 50% change in β will result in only a ~20% error in the predicted flow.

Comparison of the canopy flow and porous media approaches—Comparison of Eqs. 1 and 5 reveals that the canopy flow and porous media approaches are similar, albeit with key differences in how the resistance terms are modeled, namely, (1) the inclusion of a ''laminar resisting force'' in the porous media model, (2) the inclusion of a ''shear stress'' term in the canopy model, and (3) the way that ''form drag'' in each approach is formulated. Since the canopy approach was specifically designed for situations where flow in the canopy is high enough to be turbulent, the laminar resistance term in Eq. 5 would be negligible in comparison with the quadratic drag term. As we will show, under most wave-driven flow conditions, the shear stress term in the porous media model can be neglected since the pressure gradient is the dominant driving force. However, for long-period wave motions, the shear stress term plays an increasingly important role. Thus, to generalize the porous media model (Eq. 5) to a wider class of natural canopy flows, we can add the canopy shear stress term to the porous media model. With this addition, the only difference between the two approaches for turbulent conditions is how the form drag term is modeled.

Form drag in Eq. 1 is parameterized on the basis of calculating the drag force exerted on the canopy fluid by individual elements making up the canopy. The drag on each element is proportional to its frontal area A_f and an empirical drag coefficient C_d (note that A_f is incorporated into Eq. 1 via the frontal area parameter λ_f). This approach is very easy to apply to surfaces made up of simple bluff bodies, such as the cylinder array used by Lowe et al. (2005*b*); however, the geometry of many natural canopies (e.g., the coral canopy in Fig. 1A) is far more complex. Models of form drag resistance in the porous media approach, on the other hand, have been specifically designed to contend with the complex geometry of 3D matrices. In these formulations, form drag is parameterized as a function of the porosity and a characteristic length scale D_{eq} of the bed material. We argue that, for complex 3D bed roughness such as coral, D_{eq} can often be more readily assigned than λ_f since the frontal area A_f may be difficult to define for these complex geometries.

Another practical advantage of the porous media form drag models is that they have already been developed using a wealth of experimental data (see MEMD79) incorporating a wide range of porous bed geometries for both unidirectional and wave-driven flow conditions. For the canopy flow approach, little is known about how to predict C_d, even for a well-studied object such as a cylinder when embedded in a canopy (Ghisalberti and Nepf 2004). For wave-driven flow in submerged canopies, no direct measurements of C_d have ever been made (Lowe et al. 2005*b*). Therefore, because of the problems associated with defining λ_f and C_d for the coral used in this study, we believe that a porous media approach (modified to include the effect of the shear stress at the top of the canopy) is better suited for predicting flow through the coral canopies and is hence applied and evaluated in our study here.

Methods

Laboratory facilities and flow measurement—A detailed description of the experimental setup can be found in Lowe (2005) and is only summarized here. Experiments were conducted in a 12.5-m-long by 1.2-m-wide wave-current flume at Stanford University. Waves with a period T = 2.13 s were generated with a piston-style wave maker. The test section was filled with Porites compressa coral skeletons from Kaneohe Bay, Oahu, Hawaii, with colony diameters ranging from 10 to 30 cm and heights from 10 to 20 cm (Fig. 1). Corals were arranged in a dense canopy, which extended across the full width of the flume and 2.4 m in the streamwise x-direction (Fig. 2).

Two-dimensional velocity fields were acquired within and above the coral using particle image velocimetry (PIV). The flume was seeded with hollow glass spheres (mean diameter 11 μm) that were illuminated using a light sheet created by a Nd : YAG laser located beneath the flume test section (Fig. 3). The sheet passed through a 1.5-cm gap between the corals, a length chosen to be comparable to the ~2-cm average branch spacing measured for these *P. compressa* corals by Reidenbach et al. (2006*a*). Particles in the flow were imaged with a 12-bit CCD camera (resolution 2048 × 2048 pixels) at 15 frames s^{-1}, so that velocities were obtained at 7.5 Hz. For unidirectional flow experiments, 5000 velocity fields were acquired. For the wave experiments, a total of 8700 velocity fields were acquired at 16 equally distributed wave phases.

Image pairs were processed using MatPIV (Sveen 2004). Raw images were first processed using the Intensity Capping technique proposed by Shavit et al. (2007) and were analyzed in a sequence of four passes (subwindow sizes 64 × 64, 64 × 64, 32 × 32, and 32 × 32, each with 50% overlap). Spurious vectors were detected with a local median filter and replaced by linear interpolation. Velocities were calculated on a 127 ×

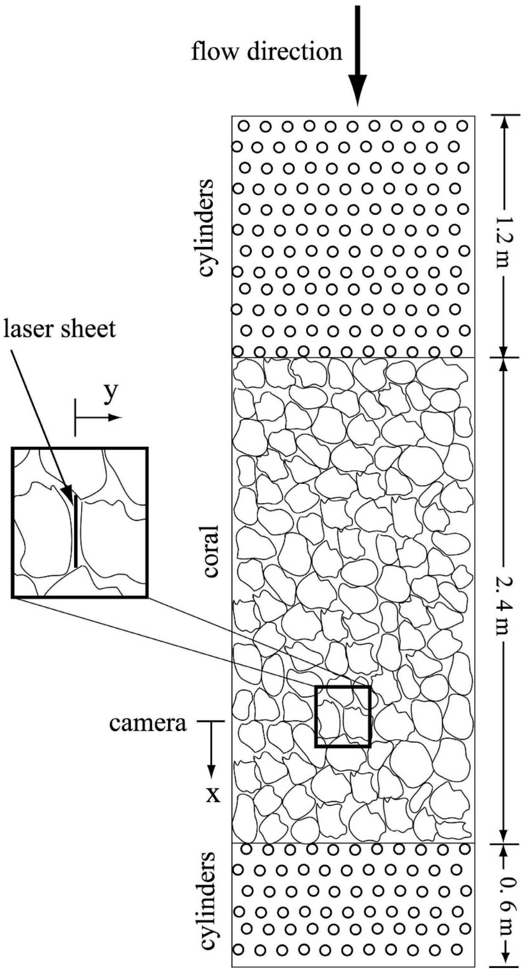

Fig. 2. The coral test section. In order to develop the boundary layer upstream and eliminate the abrupt step change in roughness at the edges of the coral canopy, arrays of vertical cylinders (height 0.1 m) used in Lowe et al. (2005*b*, 2007) were placed upstream and downstream of the coral. The passage of the laser sheet through a narrow gap in the coral roughness is shown in the enlarged diagram. Note that the x-origin is centered on the camera field of view and that the y-origin is at the lateral position of the laser sheet.

127 grid such that, given the 9.8 × 9.8-cm camera field of view, the grid resolution was 0.8 mm.

Flow conditions and coral canopy properties—Six unidirectional flow experiments were conducted (denoted U1–U6; *see* Table 1). For these experiments, the water depth was $h = 44$ cm, except in runs U3 and U4, where the effect of varying the depth was investigated. A free stream current of $U_{\infty,c} \approx 10$ cm s^{-1} was used in all runs, except U1, where the effect of varying current speed was studied. Reynolds numbers Re_h based on the channel depth varied between 22,000 and 52,000 (Table 1). To investigate the sensitivity of the flow to the particular spatial distribution of corals in the flume, three different coral arrangements were used (Table 1). Between experiments, the corals were removed and replaced in the flume in a different configuration. In arrangement 1, velocities were measured in two 9.8 × 9.8-cm image windows located above the canopy (Fig. 3A). Arrangements 2 and 3 differed from arrangement 1 in that a small gap was included in order to obtain optical access within the coral roughness; for these arrangements, three image windows were used (Fig. 3B).

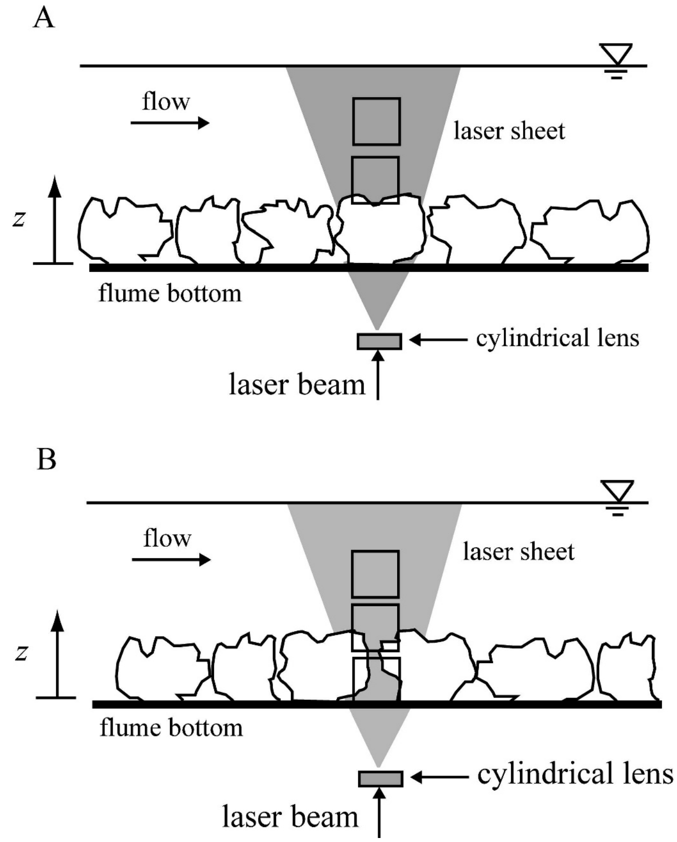

Fig. 3. View from the side of the flume showing the laser light sheet and PIV measurement windows (denoted by the boxes). (A) Setup used for coral arrangement 1, where flow was measured only above the roughness. (B) Setup used for coral arrangements 2 and 3, where flow was measured in a small gap (~2 cm) between the corals, allowing velocities to be measured within and above the coral roughness.

Three wave experiments were conducted (denoted W1–W3; *see* Table 2). For each wave experiment, a background current of $U_{\infty,c} \approx 5$ cm s^{-1} was required to minimize wave reflection at the downstream weir (Lowe et al. 2005*b*). For this general wave-current flow case, the instantaneous velocity fields u were decomposed into a current U_c, wave U_w, and turbulent velocity contribution, that is, $u = U_c + U_w + u'$. U_c is then treated as the time-averaged velocity, the wave velocity U_w is obtained by phase averaging and subtracting U_c, and the turbulent velocity contribution is the residual (*see* Lodahl et al. 1998). The waves with heights $H \approx 4$ cm produced $U_{\infty,w}^{\max} \approx 8$ cm s^{-1}. Flow conditions were the same in each wave experiments (corresponding to $\mathrm{Re}_h \sim 24{,}000$ based on $U_{\infty,w}^{rms}$) and were only distinguished by differing coral arrangements.

To accurately measure the coral canopy height near the PIV image areas, a roughness profiler was used. The profiler, similar to that used by Nunes and Pawlak (2008),

Table 1. Conditions and parameters measured directly from the unidirectional flow experiments.

Run	Coral Arrangement	h (cm)	$U_{\infty,c}$ (cm s^{-1})	Re$_h$	Re$_p$	C_f	β (m^{-1})	α_c
U1	1	44	5.2	22,000	—*	0.017±0.001	—*	—*
U2	1	44	11.1	49,000	—*	0.015±0.001	—*	—*
U3	1	35	9.6	34,000	—*	0.015±0.001	—*	—*
U4	1	28	10.6	30,000	—*	0.025±0.002	—*	—*
U5	2	44	11.8	52,000	50	0.022±0.002	19±3	0.07±0.01
U6	3	44	11.0	48,000	40	0.018±0.002	27±4	0.06±0.01

* These quantities were not calculated because no velocity measurements were made within the coral canopy for these runs.

consisted of a 110-cm-long bar with holes drilled every ~1 cm along its length. The bar was mounted above the coral, parallel to the flow direction; rods placed through the holes were used to measure the coral height to an accuracy of ±2 mm. For each coral arrangement, three of these profiles were collected at different lateral positions relative to the light sheet, one centered on the light sheet and two roughly 5 cm on either side. For each arrangement, the top of the coral canopy was characterized by the mean coral height $\bar{h}_c$ calculated along the three profiles.

The flow structure within the coral canopy should be strongly influenced by the geometric properties of the roughness. For complex natural canopies, λ_p can vary as a function of elevation z. Experiments were conducted to measure $\lambda_p(z)$ by arranging approximately 25 coral colonies into a canopy on the bottom of a rectangular box–shaped reservoir. The reservoir was filled at a known rate, and the water level h was recorded at 10 Hz to ±0.1 mm using a capacitance wire water-level gauge. By comparing the rate of water-level change dh/dt with coral absent to dh/dt measured with the coral present, the cross-sectional area occupied by the coral roughness at each elevation was estimated.

Results

Coral canopy morphology—Mean canopy heights $\bar{h}_c$ (± standard error) were 12.5 ± 0.4, 12.3 ± 0.4, and 11.9 ± 0.3 cm for coral arrangements 1, 2, and 3, respectively. Profiles of $\lambda_p(z)$ for two independent sets of corals were similar, varying between 0.1 and 0.3 within the canopy (Fig. 4). A canopy-averaged value $\bar{\lambda}_p$ can be obtained by integrating these profiles from the coral base to $\bar{h}_c$, giving $\bar{\lambda}_p$ = 0.22 ± 0.02, indicating that most of the volume in the canopy region is occupied by fluid.

Velocity profiles—Runs U1–U4, in which the flow structure was measured only above the coral canopy, were designed to investigate whether the canopy flows generated in these experiments were approximately unconfined and fully turbulent, key assumptions in the theory developed previously. Doubling the flow speed from $U_{\infty,c} \approx 5$ cm s^{-1} (run U1) to ≈ 10 cm s^{-1} (run U2) had no effect on the normalized mean velocity profile, suggesting that for flow speeds $U_{\infty,c} > 5$ cm s^{-1}, the boundary layer structure was fully turbulent (i.e., Reynolds number independent) (Fig. 5A). Decreasing the water depth from 44 cm (run U2) to 35 cm (run U3) also had no effect on the profile; however, reducing the depth to 28 cm (run U4) radically altered its shape (Fig. 5A). When the water depth decreases below 32 cm, the above-canopy flow becomes confined by the free surface (i.e., depth limited). As a result, for all experiments conducted using the default water depth (h = 44 cm), the flow structure is expected to approximate unconfined flow conditions. These observations are consistent with Nepf and Vivoni (2000), who showed that for unidirectional flow, the ratio of the shear stress to the pressure gradient scales as

$$\frac{\text{shear stress}}{\text{pressure gradient}} \sim \frac{h}{h_c} - 1 \tag{8}$$

that is, the shear layer begins to dominate the flow structure as the ratio of the water depth to canopy height increases to a point where the flow structure becomes independent of further increases in depth. Our experiments indicate that this transition occurs between h/h_c = 2.3 and 2.9.

For the unidirectional flow experiments (and when $h \geq$ 35 cm), U_c is heavily attenuated within the canopy, with a region of strong shear near the top of the canopy resulting from the vertical discontinuity in drag. Values of α_c calculated for runs U5 and U6 were 0.06–0.07 (Table 1), indicating that only a very small fraction of the momentum above the coral penetrates into the canopy. As predicted by Lowe et al. (2005*b*), much greater flow is induced within the

Table 2. Conditions and parameters measured directly from the wave experiments.

Run	Coral Arrangement	h (cm)	$U_{\infty,w}^{rms}$ (cm s^{-1})	Re$_h$	Re$_p$	C_f	β (m^{-1})	C_M	α_w
W1	1	44	5.5	24,000	—*	0.015±0.004	—*	—*	—*
W2	2	44	5.4	24,000	300	0.012±0.003	4±2	0.8±0.3	0.82±0.04
W3	3	44	5.4	24,000	300	0.016±0.004	6±3	1.0±0.3	0.78±0.04

* These quantities were not calculated because no velocity measurements were made within the coral canopy for these runs.

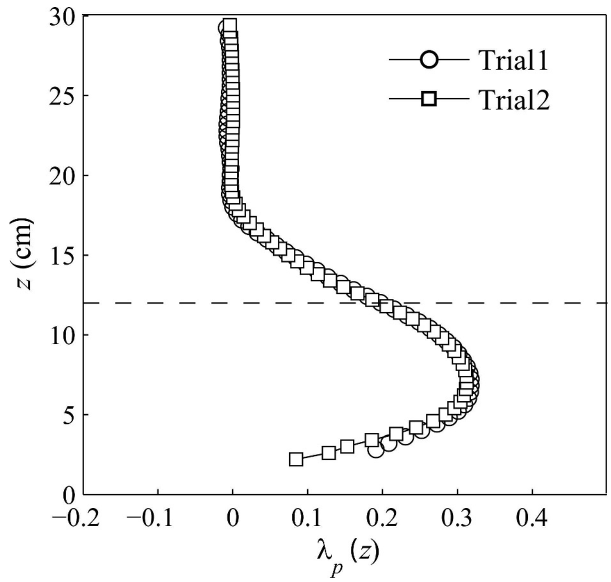

Fig. 4. Profile of $\lambda_p(z)$ calculated for two independent sets of coral colonies, representing the fractional plan area occupied by the coral at each elevation. The data were smoothed using a 2-cm vertical moving average. The dashed line denotes the mean coral height $\bar{h}_c \approx 12$ cm.

interior of the canopy in the presence of waves (Fig. 6a). Values of α_w varied between 0.78 and 0.82, where $U_{\infty,w}^{rms}$ was taken to be the magnitude of the wave velocity at the top of the wave boundary layer at $z \approx 16$ cm (Lowe et al. 2005*b*). Therefore, for these canopies and flows, surface waves generated 10 to 15 times more flow within the canopy interior than the comparable unidirectional flow.

Turbulent stresses—Profiles of the normalized Reynolds stresses above the canopy were not affected by doubling the current speed (Fig. 5B), further confirming that the boundary layer structure over the coral was fully turbulent. Likewise, decreasing the water depth from 44 to 35 cm had no effect on Reynolds stress profiles; however, decreasing the depth further to 28 cm resulted in a near doubling of the near-bed stress. Under unidirectional conditions, the normalized Reynolds stresses were nearly zero above the boundary layer, peaked slightly above the canopy height, and then diminished to approximately zero inside the canopy. These results are consistent with what is known for unidirectional canopy flows (Finnigan, 2000).

Because there was a background current present in all wave experiments, we used the phase-averaging stress approach of Lodahl et al. (1998) to decompose our turbulent Reynolds stresses into wave $\left(\overline{u'w'}\right)_w(t)$ and current components $\left(\overline{u'w'}\right)_c$. In our analysis of wave-driven flow through the coral canopy, we considered only the wave components of the mean flow and Reynolds stresses. Whereas the interaction of the background current with the wave motion might enhance the wave component of the Reynolds stress, Lodahl et al. (1998) observed no current enhancement to $\left(\overline{u'w'}\right)_w$ for cases where $U_{\infty,c}/U_{\infty,w}^{\max} < 1$. Thus, in our experiments where $U_{\infty,c}/U_{\infty,w}^{\max} \sim 0.6$, we expect our measured wave Reynolds stresses to be a good representation of those one would obtain under pure wave-driven flow. Because of the unsteady nature of the wave Reynolds stress, we characterized its magnitude with its rms value $\left|\overline{u'w'}\right|_w^{rms}$. Whereas wave-induced Reynolds stresses within canopies have not been previously reported in the literature, our normalized stresses reveal a structure that is similar to unidirectional flow (Fig. 6B). Wave

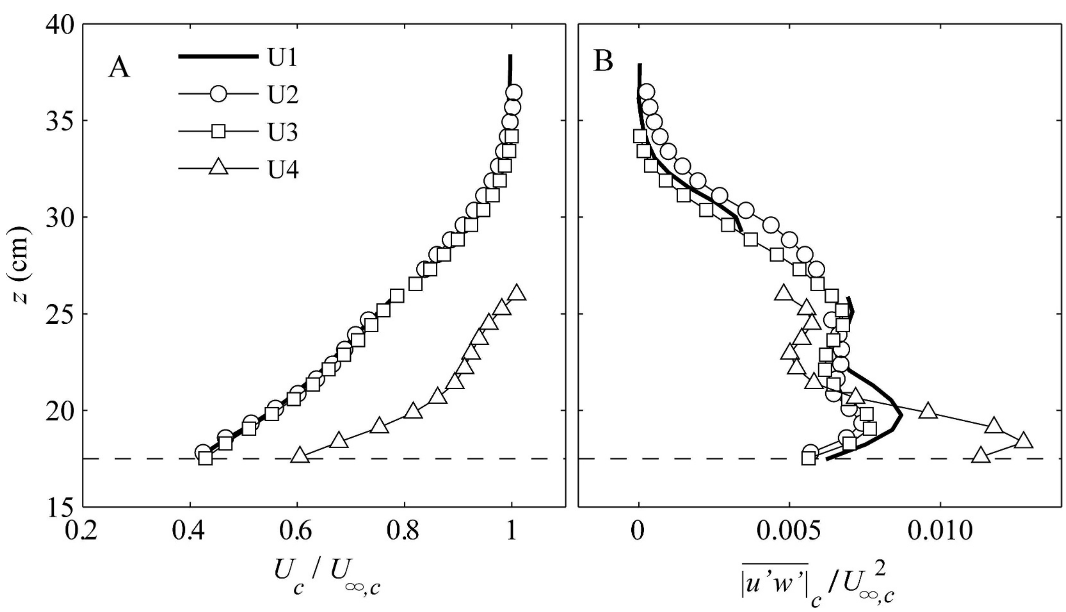

Fig. 5. Effect of flow speed and water depth on the flow structure above the coral canopy for runs U1–U4 (Table 1). (A) Mean velocity profiles. (B) Reynolds stress profiles. The horizontal dashed line denotes the local maximum coral height (below which no flow was measured for these experiments). The uncertainties in the normalized mean velocities and Reynolds stresses averaged 1×10^{-2} and 5×10^{-4}, respectively.

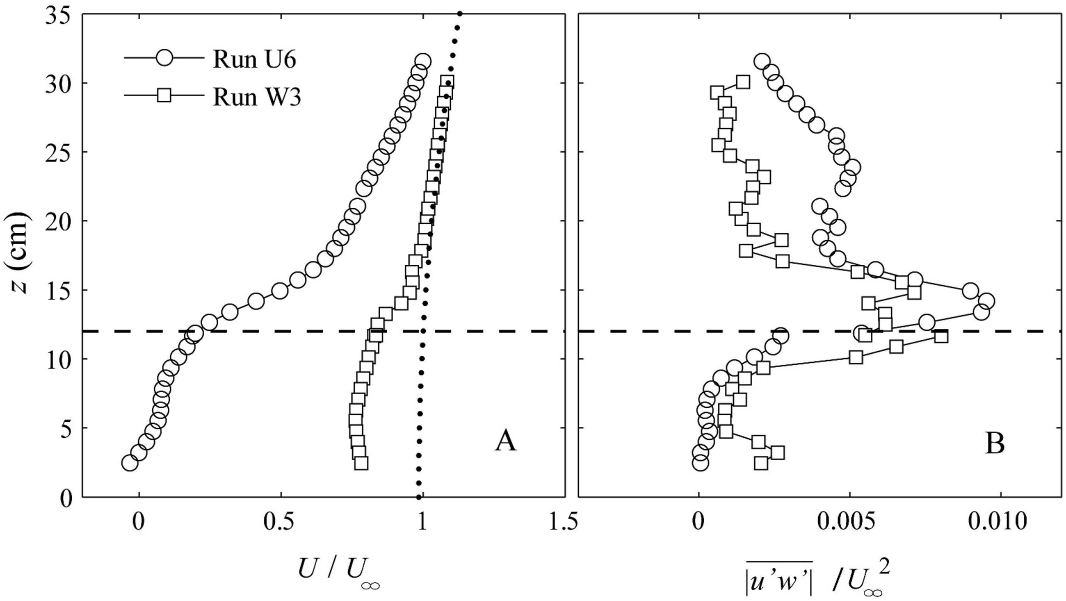

Fig. 6. (A) Normalized current $U_c/U_{\infty,c}$ and wave $U_w^{rms}/U_{\infty,w}^{rms}$ mean velocity profiles for runs U6 and W3, respectively. The vertical dotted line represents the predicted attenuation of the $U_{\infty,w}^{rms}$ based on linear wave theory with the coral absent. The uncertainties in the normalized mean velocities are 1×10^{-2} for both waves and currents. The horizontal dashed line denotes the mean coral height $\bar{h}_c$. (B) The corresponding normalized Reynolds stress profiles associated with the unidirectional $\left|\overline{u'w'}\right|_c / U_{\infty,c}^2$ and wavy $\left|\overline{u'w'}\right|_w^{rms} / \left(U_{\infty,w}^{rms}\right)^2$ flows. The uncertainties in the normalized Reynolds stresses averaged 5×10^{-4} and 2×10^{-3} for runs U6 and W3, respectively.

Reynolds stresses are small in the canopy and peak near the canopy height. Above the wave boundary layer ($z \approx$ 15 cm), where net viscous forces are small, wave-induced Reynolds stresses approach zero. Thus, Reynolds stress profiles under both unidirectional and oscillatory flows indicate that a region of intense turbulent mixing forms at the canopy interface ($z \approx$ 10–16 cm), where peak normalized Reynolds stresses are 0.005–0.012.

Direct estimation of model parameters from PIV measurements: Bed shear stresses τ_c for unidirectional flow are parameterized using a quadratic friction law based on a friction coefficient C_f and the free stream velocity $U_{\infty,c}$, that is,

$$\tau_c = \frac{1}{2}\rho C_f U_{\infty,c}^2 \qquad (9)$$

thus consistent with how the "shear stress" term is formulated in Eq. 1. Following Kastner-Klein and Rotach (2004), τ_c can be estimated from the peak Reynolds stress in each profile (Fig. 6B) according to $\tau_c \approx \rho\left|\overline{u'w'}\right|_{\max}$. Thus, an estimate of C_f was obtained for each unidirectional flow (Table 1) and averaged $C_f = 0.018$ for unconfined experiments (runs U1–U3, U5, and U6).

For turbulent, unidirectional flows with depth limitation, Eq. 5 implies that the force balance on the volume of water $A_T h_c(1 - \lambda_p)$ moving through the canopy of plan area A_T is

$$\left[-\frac{1}{\rho}\frac{dP}{dx} + \frac{\tau_c}{\rho h_c}\right] A_T h_c\left(1 - \lambda_p\right) = \beta U_c^2 A_T h_c\left(1 - \lambda_p\right) \qquad (10)$$

The pressure gradient can be estimated by considering the momentum balance above the canopy, that is, $-dP/dx = \tau_c/(h - h_c)$. Combining this with Eq. 10 gives an expression relating β to measured values of τ_c and $\hat{U}_c$:

$$\beta = \frac{\left|\overline{u'w'}\right|_{\max}}{h_c \hat{U}_c^2}\left(\frac{1}{1 - h_c/h}\right) \qquad (11)$$

Using Eq. 11, β was determined to be 19 ± 3 and 27 ± 4 m^{-1} for runs U5 and U6, respectively.

Canopy shear stresses (and thus C_f) under oscillatory flow can be estimated from $U_{\infty,w}^{rms}$ and by finding the peak in the Reynolds stress profile as was done under unidirectional flow using Eq. 9 (Sleath 1987). From this approach, C_f averaged 0.014 for runs W1–W3 (Table 2). These values are similar to those calculated under unidirectional flow (Table 1).

In the presence of waves, both inertial and drag forces attenuate flow within the canopy interior. Thus, both β and C_M must be simultaneously estimated from the flow data. For our experiments, form drag dominates over laminar resistance since $\mathrm{Re}_p \sim 300$, so the latter can be neglected from Eq. 5. This leaves us with three terms that can be directly measured (acceleration, pressure gradient, shear) and the two force terms that must be estimated (inertial, drag). Shear stress time series were estimated from measured C_f. Flow accelerations within the canopy interior were estimated by numerically differentiating the canopy depth-averaged ($z < \bar{h}_c$) velocities (Fig. 7). Similarly, the large-scale wave pressure gradients were calculated via

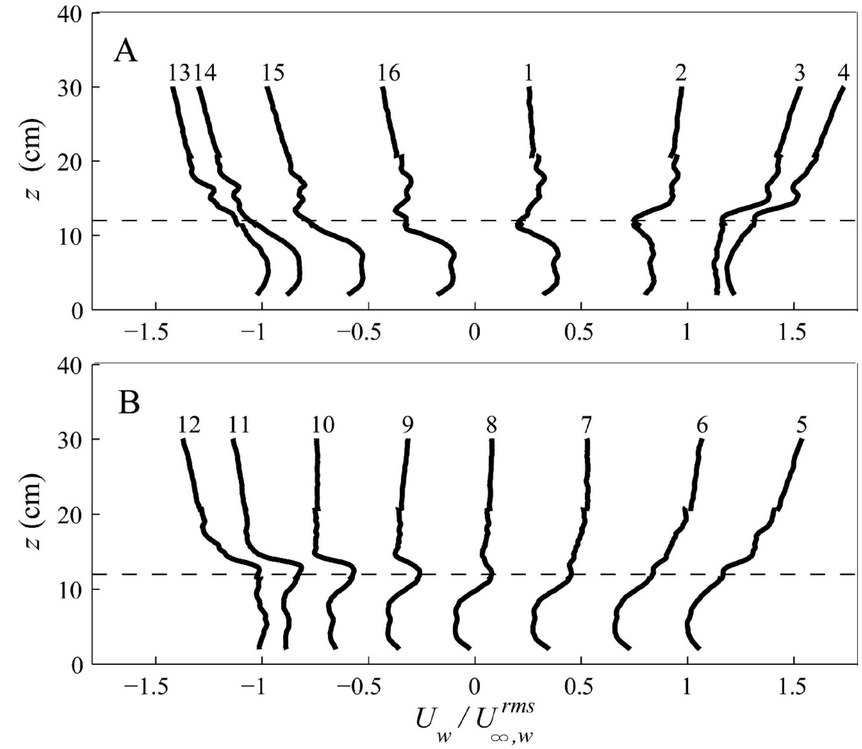

Fig. 7. Phase-dependent profiles of the horizontal wave velocity U_w for run W3. Each profile number corresponds to a different wave phase (22.5 degrees apart). (A) Profiles undergoing a positive acceleration (moving to the right). (B) Profiles undergoing a negative acceleration (moving to the left). Note the phase difference between the in- and above-canopy flow as a result of canopy form drag. The dashed line denotes the mean coral height $\bar{h}_c$.

Eq. 3, using the flow accelerations computed based on numerically differentiating $U_{\infty,w}(t)$. The two unknown coefficients β and C_M were then calculated from the observed flow attenuation within the canopy over a wave cycle. To do this, we sought values for β and C_M that would minimize the difference in both amplitude and phase between the observed and modeled in-canopy flow time series. From this analysis, for run W2 we obtained β and C_M values of 4 ± 2 and 0.8 ± 0.3 m^{-1}, respectively, and for run W3 values of 6 ± 3 and 1.0 ± 0.3 m^{-1}, respectively (Table 2). We note that these β are somewhat lower than measured under unidirectional flow; some possible sources of this discrepancy are addressed later.

Estimation of model parameters from the literature—For unconfined, unidirectional, fully rough flow, values of C_f should be a function only of the morphological properties of the bed (Boudreau and Jørgensen 2001). Reidenbach et al. (2006*b*) observed values of C_f = 0.018–0.030 over coral reef communities for unidirectional flow in the Red Sea. This value is consistent with the C_f = 0.02–0.03 measured for a model canopy by Lowe et al. (2005*b*) as well as values of $C_f = O(0.01)$ reported in other canopy flow studies (*see* Grimmond and Oke 1999 for a review). Therefore, it appears that assuming $C_f = O(0.01)$ provides a surprisingly robust parameterization of shear stresses generated by unidirectional flow over many benthic canopies, which is an order of magnitude larger than the $C_f = O(0.001)$ often observed over smooth beds (Feddersen et al. 2003).

For wave-driven flows, various authors have reported values for C_f that are much larger than for unidirectional flow. For example, field studies over coral reefs give values of C_f in the range of 0.15–0.3 (Nelson 1996; Falter et al. 2004; Lowe et al. 2005*a*). Likewise, values of C_f for wave-driven flow over other rough surfaces have generally been found to be $O(0.1)$ (e.g., Nielsen 1992), similar to the magnitude of C_f observed over reefs. This suggests that C_fs for wavy flows over rough walls can be an order of magnitude larger than for unidirectional flows.

For porous media flows, K_p and β can be estimated from Eqs. 6 and 7 based on simple morphological properties of the bed (D_{eq}, λ_p). Although our coral canopies may be more complex geometrically than some porous media, studies of flow resistance through randomized cylindrical fiber mats have related D_{eq} to 1.5 times the fiber diameter (MEDM79). Thus, for our coral canopies we assumed D_{eq} = 2.7 ± 0.9 cm based on the average branch diameter D_{cyl} = 1.8 ± 0.6 cm measured for the same *P. compressa* community used in our study (Reidenbach et al. 2006*a*). Substituting this value with λ_p = 0.22 ± 0.02 into Eqs. 6 and 7 predicts that K_p and β will be (4.0 ± 2.4) × 10^{-5} m^2 and 19 ± 7 m^{-1}, respectively, for our coral canopy.

There are not many estimates of C_M reported in the literature, particularly for canopies as morphologically complex as our coral community. Both Van Gent (1995)

Table 3. Sensitivity of the model to the model parameters for three different flow conditions (expressed in terms of the wave excursion length A_∞). α_{w0} is the default value based on $\lambda_p = 0.22$, $C_f = 0.02$, $\beta = 19$ m^{-1}, $C_M = 1$, and $K_p = 4.0 \times 10^{-5}$ m^2. A table value of 0.5 indicates that for a 1% change in the parameter, there is a 0.5% change in α_w. An asterisk (*) indicates that values are not truly zero but are so small as to be neglected. Note that laminar resistance (last column) is negligible under all flow conditions.

	α_{w0}	$\frac{\lambda_p}{\alpha_w}\frac{\partial\alpha_w}{\partial\lambda_p}$	$\frac{C_f}{\alpha_w}\frac{\partial\alpha_w}{\partial C_f}$	$\frac{\beta}{\alpha_w}\frac{\partial\alpha_w}{\partial\beta}$	$\frac{C_M}{\alpha_w}\frac{\partial\alpha_w}{\partial C_M}$	$\frac{K_p}{\alpha_w}\frac{\partial\alpha_w}{\partial K_p}$
$A_\infty \rightarrow \infty$ (unidirectional)	0.07	0.00	0.50	0.50	0.00	0.00*
$A_\infty \rightarrow 0$ (inertial dominated)	0.78	0.28	0.00	0.00	0.22	0.00
$A_\infty = 0.5$ m (intermediate)	0.32	0.05	0.00*	0.39	0.04	0.00*

and Gu and Wang (1991) found a best estimate of $C_M \sim 0.5$, whereas Hannoura and Mccorquodale (1978) measured values as high as $C_M \sim 2$. Lowe et al. (2005*b*) found that $C_M = 1.5$ gave the best agreement for modeling oscillatory flow through a staggered array of cylinders. Given the relatively large scatter in these values of C_M, a value of 1 ± 0.5 is consistent with the literature.

Sensitivity of the model to parameter values—We investigated the sensitivity of the model to its various parameters by examining how the ratio of the in-canopy flow speed to the free-stream flow speed, α, changes with each parameter value (Table 3). Under quasi-unidirectional flow (i.e., $A_\infty \rightarrow \infty$), the critical variables for determining α are both C_f and β since the dominant momentum balance is between the shear stress and drag terms. Not surprisingly, for inertial-dominated flow ($A_\infty \rightarrow 0$), λ_p and C_M are the dominant variables affecting α; however, the sensitivity of α to these parameters is less than on C_f and β for unidirectional flow. This is notable since the relatively large 50% scatter in reported values of C_M will result in only a ~10% error in predicted α. Under intermediate conditions (e.g., $A_\infty = 0.5$ m), where both drag and inertial forces are important, α is most affected by differences in β and only marginally sensitive to variations in λ_p or C_M (Table 3). Finally, it is important to note the lack of sensitivity of α to variations in K_p under all flow conditions; hence, for the coral canopy and flow conditions used in the experiments, the contribution of laminar resistance in Eq. 5 can indeed be neglected in our application.

Discussion

Comparison between observed and predicted parameter values—Values of $C_f \approx 0.02$ measured under unidirectional flow are consistent with the $C_f = O(0.01)$ generally observed over canopies (Grimmond and Oke 1999). Measured C_fs associated with turbulent wave stresses were comparable to the unidirectional values (~0.02). At first this appears to contradict the value $C_f \approx 0.2$ cited for reefs under wavy conditions (see the previous discussion). However, this discrepancy can be explained by the fact that these values were inferred from observations of wave dissipation over sections of reef. For wavy flows through canopies, dissipation by drag forces will dominate over bed shear such that these reported values will incorporate the combined effect of both processes. Given that our model explicitly differentiates between dissipation resulting from drag and shear stresses, a value $C_f \sim 0.02$ appears to be appropriate for parameterizing the contribution from the wave-induced shear layer alone. It is important to emphasize that C_f is an important determinant of α only in the limit of unidirectional flow (Table 3). Thus, only for unidirectional flow would it be necessary to make accurate estimates of C_f for a given canopy. Given that C_f typically falls between 0.015 and 0.025, assuming $C_f = 0.02$ is likely to lead to uncertainties in α of only 12% (Table 3). Thus, an a priori estimation of C_f may be acceptable, depending on how accurately the mean flow within the canopy needs to be predicted.

Direct estimates of β under unidirectional flow yielded values (19 ± 3 and 27 ± 4 m^{-1}) that were close to those predicted from the literature based solely on the measured morphological properties of the canopy (19 ± 7 m^{-1}, Eq. 7). The ability of porous media relationships to make robust estimates of β is, thus, a good reason to use them in a hybridized model describing flow in natural canopies. At present, a similarly straightforward approach for determining form drag parameter values for even idealized canopy geometries does not yet exist in the canopy literature (*see* discussion in Ghisalberti and Nepf 2004). Prior studies have found that β is comparable if not higher under wavy flow than under purely unidirectional flow (e.g., Van Gent 1995). Our values of β under wavy flow were somewhat lower than those calculated under unidirectional flow. This discrepancy may be due to our wave experiments having been conducted close to the inertia-dominated limit of very small A_∞. As such, the contribution of drag should be minimal, making the determination of β from the observed momentum balance difficult. Nonetheless, using values of β determined under unidirectional flow for modeling wavy canopy flow should be reasonable given that under intermediate flow conditions, even a 30% uncertainty in β will result in only a 10% uncertainty in α (Table 3).

The values of $C_M \sim 1$ were within the range cited in the literature (0.5–2). We expect that intermediate flow conditions best represent many natural canopies living in the presence of random waves, with the exception of those exposed to short-period wind waves. Given the insensitivity of α to C_M under intermediate flow conditions (Table 3), we

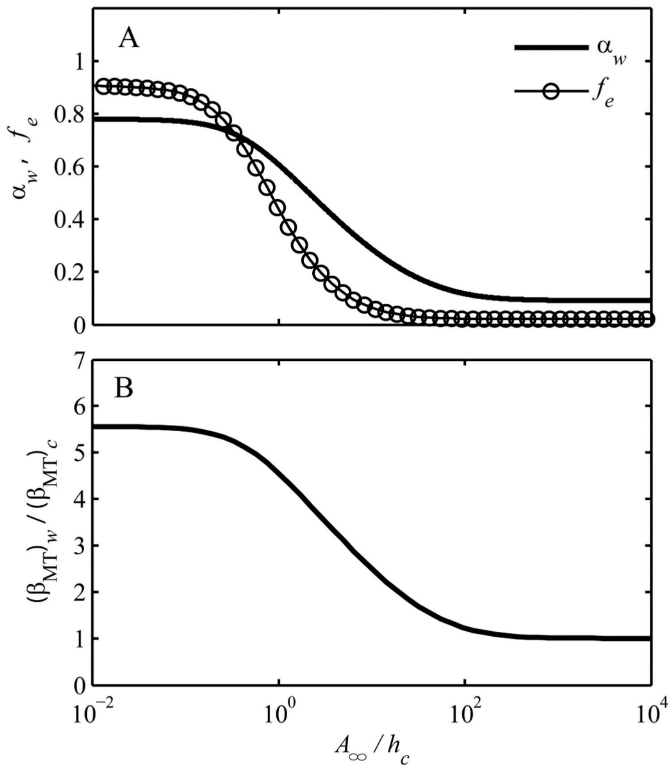

Fig. 8. (A) α_w predicted from the model (Eq. 5) assuming typical coral canopy values $C_f = 0.02$, $\beta = 10$ m^{-1}, and $C_M = 1$, as a function of the normalized wave excursion length A_∞, with the corresponding f_e calculated via Eq. 13 superimposed. Uncertainty in α_w arising from the model input parameters ranges between 0.09 for $A_\infty/h_c << 1$ to 0.02 for $A_\infty/h_c >> 1$, while uncertainty in f_e ranges from 0.3 to 0.002 between the same limits. (B) Normalized mass transfer coefficients inferred from Eq. 14, expressed as the mass transfer coefficient associated with waves $(\beta_{MT})_w$ normalized by the corresponding unidirectional value $(\beta_{MT})_c$. Uncertainty in the normalized mass transfer coefficients, due to uncertainties in α_w, ranges from 0.9 for $A_\infty/h_c << 1$ to zero (by definition) for $A_\infty/h_c >> 1$.

suggest that assuming $C_M \approx 1$ should be an acceptable approximation for most canopies under most wave conditions.

Finally, we compare our observed α's with model predictions. For unidirectional flow, Eq. 5 predicts $\alpha_c = (C_f/2\beta\bar{h}_c)^{0.5}$ (*see* Lowe et al. 2005*b*). By assigning model parameter values predicted solely from the literature (i.e., $C_f = 0.02$, $C_M = 1$, and $\beta = 19$ m^{-1} from Eq. 7 using measured D_{eq} and λ_p), the predicted $\alpha_c = 0.07$ agrees with our measurements to within statistical certainty (Table 1). Under wavy flow, the numerical solution of Eq. 5 predicts $\alpha_w = 0.73$, a value only ~10% less than observed (Table 2). Most important, the model predicts that α for our wave experiments will be an order of magnitude greater than for unidirectional flow, reiterating that the model captures the physical mechanisms responsible for the enhanced flow that has been observed in all previous studies of wave-driven flow in canopies. Finally, we can use the model to predict how α will vary over a range of different wave conditions, that is, by varying A_∞ (Fig. 8A). We see that α attains a maximum (inertial-force dominated) value of $\alpha = 0.78$ for small A_∞s and decreases toward a minimum (unidirectional) flow value of $\alpha = 0.07$ for large A_∞s.

Model applications—Conventional models of dissipation ε_{bf} generated by "bottom friction" over rough bottoms do not explicitly model flow within the bed roughness or canopy elements (e.g., Jonsson 1966). These models predict a cubic dependency on velocity, which results from the quadratic bottom stress formulation (Eq. 9), based on the near-bottom velocity U_∞ (Nielsen 1992), that is,

$$\varepsilon_{bf} = \frac{2}{3\pi}\rho f_e U_\infty^3 \tag{12}$$

where f_ε is termed an "energy dissipation factor." It is clear from our model that as flow changes from unidirectional to inertial dominated, the amount of dissipation occurring in the canopy can dramatically increase as more flow passes through the canopy and form drag begins to dominate over bed shear. Thus, f_ε can change for constant U_∞, depending on the degree to which waves penetrate into the canopy following the relationship derived by Lowe et al. (2007):

$$f_e = C_f + 2\beta h_c\left(1 - \lambda_p\right)\alpha^3 \tag{13}$$

where the $C_d\lambda_f$ in the Lowe et al. (2007) expression is replaced with $2\beta h_c(1 - \lambda_p)$ in accordance with the porous media formulation we are using here. As an example, for typical values of C_f and β for our coral canopy, Eq. 13 predicts that f_ε can be as large as $O(1) >> C_f$ under wavy conditions (Fig. 8A), implying that for a wavy flow, dissipation by drag forces will dominate over shear stresses that form at the canopy interface.

Prior work on mass transfer of nutrients to coral communities for *unidirectional* flow show a dependency of the mass transfer coefficient β_{MT} on $U_\infty^{0.8}$ (Bilger and Atkinson 1992). Rates of whole-canopy mass transfer appear to be driven primarily by the mean in-canopy flow speed under both unidirectional and oscillatory flow (Lowe et al. 2005*c*; Falter et al. 2007). If we assume a similar dependency of β_{MT} on flow within the canopy $\hat{U}$, then

$$\beta_{MT} \propto \hat{U}^{0.8} \propto \alpha^{0.8} U_\infty^{0.8} \tag{14}$$

This implies that the mass transfer of nutrients to the community can change for the same U_∞ when the flow goes from small α in unidirectional flow to large α in wavy flows. Fig. 8B predicts that under wavy conditions, mass transfer rates can be enhanced by more than five times over the corresponding unidirectional flow value. Moreover, given that dissipation of wave energy (via the parameter f_ε) is also controlled by α (Eq. 13), we expect that whole community mass transfer rates are correlated with total rates of dissipation (Falter et al. 2004).

It is clear from this study that existing flow parameterizations based on porous media theory can be used to predict flow inside canopies. The strength of existing empirical porous media drag parameterizations (Eq. 7) is that model parameters can often be calculated from simpler metrics of the canopy morphology than with present canopy-flow parameterizations, when the bed material is complex and 3D. An additional benefit is that empirical relationships between model parameters have already been developed from a wealth of data on flow in complex porous matrices with widely differing morphologies. However, the accuracy of predicted α still depends on how accurately the model parameters (i.e., β and C_M) can be estimated. Although existing parameterizations appear to work well for our coral canopies, to know how accurately these formulations parameterize resistance for a more diverse range of biological canopy morphologies (e.g., those formed by seagrass, kelp, and so on) will require additional testing. Nonetheless, it should eventually be possible to model mean flow in natural canopies at a large-scale (tens to hundreds of meters) using the porous media approach based on (1) in situ estimates of the canopy morphology parameters and (2) measurements of free-stream flow conditions without the need for detailed measurements of flow dynamics within the canopy interior. Once validated in the field, our canopy/porous media model could be used to estimate rates of dissipation and nutrient uptake in natural canopies, thereby improving our ability to model the physical and ecological dynamics of the benthos.

References

Ackerman, J. D., and A. Okubo. 1993. Reduced mixing in a marine macrophyte canopy. Funct. Ecol. **7:** 305–309.

Adams, P. N., R. S. Anderson, and J. Revenaugh. 2002. Microseismic measurement of wave-energy delivery to a rocky coast. Geology **30:** 895–898.

Atkinson, M. J., and R. W. Bilger. 1992. Effects of water velocity on phosphate uptake in coral reef-flat communities. Limnol. Oceanogr. **37:** 273–279.

Bear, J. 1972. Dynamics of fluids in porous media. Elsevier.

Bilger, R. W., and M. J. Atkinson. 1992. Anomalous mass transfer of phosphate on coral reef flats. Limnology and Oceanography **37:** 261–272.

Boudreau, B. P., and B. B. Jørgensen. 2001. The benthic boundary layer: Transport processes and biogeochemistry. Oxford University Press.

Britter, R. E., and S. R. Hanna. 2003. Flow and dispersion in urban areas. Annu. Rev. Fluid Mech. **35:** 469–496.

Carpenter, R. C., J. M. Hackney, and W. H. Adey. 1991. Measurements of primary productivity and nitrogenase activity of coral-reef algae in a chamber incorporating oscillatory flow. Limnol. Oceanogr. **36:** 40–49.

Dean, R. G., and R. A. Dalrymple. 1991. Water wave mechanics for engineers and scientists. World Scientific.

Engelund, F. 1953. On the laminar and turbulent flows of ground water through homogeneous sand. Trans. Danish. Acad. Tech. Sci **3:** 1.

Falter, J. L., M. J. Atkinson, R. J. Lowe, S. G. Monismith, and J. R. Koseff. 2007. Effects of non-local turbulence on the mass transfer of dissolved species to reef corals. Limnol. Oceanogr. **52:** 274–285.

———, ———, and M. A. Merrifield. 2004. Mass transfer limitation of nutrient uptake by a wave-dominated reef flat community. Limnol. Oceanogr. **49:** 1820–1831.

Feddersen, F., E. L. Gallagher, R. T. Guza, and S. Elgar. 2003. The drag coefficient, bottom roughness, and wave-breaking in the nearshore. Coast. Eng. **48:** 189–195.

Finnigan, J. 2000. Turbulence in plant canopies. Annu. Rev. Fluid Mech. **32:** 519–571.

Ghisalberti, M., and H. M. Nepf. 2002. Mixing layers and coherent structures in vegetated aquatic flow. J. Geophys. Res. **107:** 1–11.

———, and ———. 2004. The limited growth of vegetated shear flows. Water Resour. Res. **40:** W07502, doi:07510.01029/02003WR002776.

Grimmond, C. S. B., and T. R. Oke. 1999. Aerodynamic properties of urban areas derived from analysis of surface form. J. Appl. Meteorol. **38:** 1262–1292.

Gu, Z. H., and H. Wang. 1991. Gravity-Waves over Porous Bottoms. Coast. Eng. **15:** 497–524.

Hannoura, A. A., and I. A. Mccorquodale. 1978. Virtual mass of coarse granular media. J. Waterways Port Coast. Eng. Div. ASCE **104:** 191–200.

Jonsson, I. G. 1966. Wave boundary layers and friction factors,, Proceedings of the Tenth Conference on Coastal Engineering, ASCE.

Kastner-Klein, P., and M. W. Rotach. 2004. Mean flow and turbulence characteristics in an urban roughness sublayer. Boundary Layer Meteorology **111:** 55–84.

Lesser, M. P., V. M. Weis, M. R. Patterson, and P. L. Jokiel. 1994. Effects of morphology and water motion on carbon delivery and productivity in the reef coral, *Pocillopora damicornis* (Linnaeus)—diffusion-barriers, inorganic carbon limitation, and biochemical plasticity. J. Exp. Mar. Biol. Ecol. **178:** 153–179.

Lodahl, C. R., B. M. Sumer, and J. Fredsoe. 1998. Turbulent combined oscillatory flow and current in a pipe. J. Fluid Mech. **373:** 313–348.

Lowe, R. J. 2005. The effect of surface waves on mass and momentum transfer processes in shallow coral reef systems. Ph.D. dissertation. Stanford Univ.

———, J. L. Falter, M. D. Bandet, G. Pawlak, M. J. Atkinson, S. G. Monismith, and J. R. Koseff. 2005*a*. Spectral wave dissipation over a barrier reef. J. Geophys. Res. Oceans **110:** C04001, doi:10.1029/2004JC002711.

———, ———, J. R. Koseff, S. G. Monismith, and M. J. Atkinson. 2007. Spectral wave flow attenuation within submerged canopies: implications for wave energy dissipation. J. Geophys. Res. **112:** C05018, doi:10.1029/2006JC003605.

———, J. R. Koseff, and S. G. Monismith. 2005*b*. Oscillatory flow through submerged canopies. Part 1. Velocity structure. J. Geophys. Res. **110:** C10016, doi:10.1029/2004JC002788.

———, ———, ———, and J. L. Falter. 2005*c*. Oscillatory flow through submerged canopies. Part 2. Canopy mass transfer. J. Geophys. Res. **110:** C10017, doi:10.1029/2004JC002789.

Macdonald, I. F., M. S. Elsayed, K. Mow, and F. A. L. Dullien. 1979. Flow through porous-media—Ergun equation revisited. Ind. Eng. Chem. Fundam. **18:** 199–208.

Mcdonald, C. B., J. R. Koseff, and S. G. Monismith. 2006. Effects of the depth to coral height ratio on drag coefficients for unidirectional flow over coral. Limnol. Oceanogr. **51:** 1294–1301.

Mendez, F. J., and I. J. Losada. 2004. An empirical model to estimate the propagation of random breaking and nonbreaking waves over vegetation fields. Coast. Eng. **51:** 103–118.

Nelson, R. C. 1996. Hydraulic roughness of coral reef platforms. Appl. Ocean Res. **18:** 265–274.

Nepf, H. M., and E. R. Vivoni. 2000. Flow structure in depth-limited, vegetated flow. J. Geophys. Res. **105:** 28547–28557.

NIELSEN, P. 1992. Coastal bottom boundary layers and sediment transport. World Scientific.

NOWELL, A. R. M., AND M. CHURCH. 1979. Turbulent flow in a depth-limited boundary layer. J. Geophys. Res. **84:** 4816–4824.

NUNES, V., AND G. PAWLAK. 2008. Observations of physical roughness over a coral reef. J. Coast. Res. **24:** 39–50.

OLDHAM, C. E., AND J. J. STURMAN. 2001. The effect of emergent vegetation on convective flushing in shallow wetlands: Scaling and experiments. Limnol. Oceanogr. **46:** 1486–1493.

RAUPACH, M. R., R. A. ANTONIA, AND S. RAJAGOPALAN. 1991. Rough-wall turbulent boundary layers. Appl. Mech. Rev. **44:** 1–25.

REIDENBACH, M. A., J. R. KOSEFF, S. G. MONISMITH, J. V. STEINBUCK, AND A. GENIN. 2006a. The effects of waves and morphology on mass transfer within branched reef corals. Limnol. Oceanogr. **51:** 1134–1141.

———, S. G. MONISMITH, J. R. KOSEFF, G. YAHEL, AND A. GENIN. 2006b. Boundary layer turbulence and flow structure over a fringing coral reef. Limnol. Oceanogr. **51:** 1956–1968.

SCHLICHTING, H., AND K. GERSTEN. 2000. Boundary-layer theory. Springer.

SHAVIT, U., R. J. LOWE, AND J. V. VITTORIO. 2006. Intensity capping: A simple method to improve cross-correlation PIV results. Exp. Fluids **42:** 225–240, doi:10.1007/s00348-006-0233-7.

SLEATH, J. F. A. 1987. Turbulent oscillatory flow over rough beds. J. Fluid Mech. **182:** 369–409.

SOLLITT, C. K., AND R. H. CROSS. 1972. p. 1827–1846. Wave transmission through permeable breakwaters, Proceedings of the 13th ASCE Conference on Coastal Engineering.

SVEEN, J. K. 2004. An introduction to MatPIV v1.6.1, Dept. of Math, University of Oslo. Available from http://www.math.uio.no/~jks/matpiv

VAN GENT, M. R. A. 1995. Porous flow-through rubble-mound material. J. Waterway Port Coast. Ocean Eng. ASCE **121:** 176–181.

WARD, J. C. 1964. Turbulent flow in porous media, p. 1–12. Proceedings of the ASCE Hydraulic Division.

WHITAKER, S. 1996. The Forchheimer equation: A theoretical development. Transport Porous Media **25:** 27–61.

WU, F. C., H. W. SHEN, AND Y. J. CHOU. 1999. Variation of roughness coefficients for unsubmerged and submerged vegetation. J. Hydraulic Eng. ASCE **125:** 934–942.

Received: 14 May 2007
Accepted: 30 May 2008
Amended: 12 June 2008